2017

Palladium Nanoparticles Supported on Ce-Metal–Organic Framework for Efficient CO Oxidation and Low-Temperature CO2 Capture

Andrew Lin
Virginia Commonwealth University

Amr Awad Ibrahim
Virginia Commonwealth University

Pezhman Arab
Virginia Commonwealth University

Hanii M. El-Kaderi
Virginia Commonwealth University

M. Samy El-Shall
Virginia Commonwealth University, mselshal@vcu.edu

Follow this and additional works at: http://scholarscompass.vcu.edu/chem_pubs

Part of the Chemistry Commons

Palladium Nanoparticles Supported on Ce-Metal–Organic Framework for Efficient CO Oxidation and Low-Temperature CO2 Capture

Andrew Lin,[†] Amr Awad Ibrahim,[†,‡] Pezhman Arab,[†] Hani M. El-Kaderi,[†] and M. Samy El-Shall*,[†]

[†]Department of Chemistry Virginia Commonwealth University Richmond, Virginia 23284-2006, United States
[‡]Department of Chemistry, Faculty of Science, Mansoura University, Al-Mansoura, Egypt

S Supporting Information

ABSTRACT: In this article, we report the lowest-temperature CO oxidation catalyst supported on metal–organic frameworks (MOFs). We have developed a facile, general, and effective approach based on microwave irradiation for the incorporation of Pd nanoparticle catalyst within Ce-MOF. The resulting Pd/Ce-MOF material is a unique catalyst that is capable of CO oxidation at modest temperatures and also of efficient uptake of the product CO_2 gas at low temperatures. The observed catalytic activity of this material toward CO oxidation is significantly higher than those of other reported metal nanoparticles supported on MOFs. The high activity of the Pd/Ce-MOF catalyst is due to the presence of Ce(III) and Ce(IV) ions within the metal–organic framework support. The Pd nanoparticles supported on the Ce-MOF store oxygen in the form of a thin palladium oxide layer at the particle–support interface, in addition to the oxygen stored on the Ce(III)/Ce(IV) centers. Oxygen from these reservoirs can be released during CO oxidation at 373 K. At lower temperatures (273 K), the Pd/Ce-MOF has a significant CO_2 uptake of 3.5 mmol/g.

KEYWORDS: palladium nanoparticles, cerium-MOF, CO oxidation, CO_2 uptake, heterogeneous catalysis, Pd catalyst supported on Ce-MOF
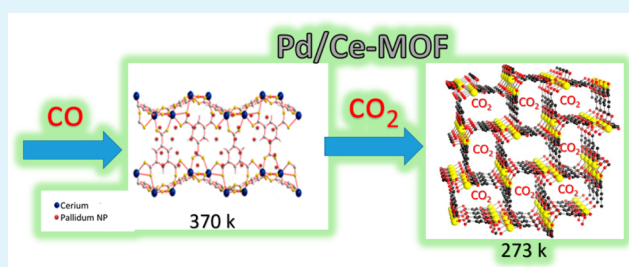
INTRODUCTION

Metal–organic frameworks (MOFs) are a new class of highly porous crystalline materials with well-defined cavities or channels that can accommodate a variety of guest species of different sizes and shapes for a variety of applications in gas storage, separations, and heterogeneous catalysis.[1−6] The interest in MOFs as catalyst supports arises from their unusually large surface areas, well-ordered crystalline structures, high porosities, tunable pore sizes, and modifiable surface properties.[1−6] MOFs provide several ways to incorporate catalysts through their centers with unsaturated coordination sites, metal nanoparticles encapsulated within the pores, and catalytic sites inherent in the structures of the frameworks.[1−6]

The catalytic activities of several MOF-based catalysts have been demonstrated for liquid-phase reactions such as cyanosilylation, hydrogenation, polymerization, and isomerization,[7−10] as well as for enantioselective separations, organic transformations for the production of chemicals,[11,12] oxygen reduction reactions in fuel cells,[13,14] and photocatalytic hydrogen production.[13,15,16] In contrast to liquid-phase reactions, only a few gas-phase reactions and gas–solid reactions using MOF-based catalysts have been investigated. For example, a few reports exist on the use of MOF-based catalysts for CO oxidation.[3,4,17−21] This reaction has significant health, industrial, and environmental impacts because of the

toxicity of CO[22] and the need to remove it from indoor air and from the H_2 streams used for the fuel-cell applications because of its poisoning effect on the performance of fuel cells.[23] Although catalytic oxidation is considered to be the most effective method for the removal of CO, the generation of CO_2 creates another serious concern, given that CO_2 capture and sequestration (CCS) remains a central technique for mitigating global warming and climate changes. Therefore, the development of low-temperature CO oxidation catalysts that are also capable of efficient CO_2 capture is of immense interest for a variety of applications such as improving fuel-cell performance, removing toxic gases released into the atmosphere by combustion and automotive exhaust processes, and meeting stringent environmental regulations for the treatment of air pollutants.[24−26]

In this article, we report on the development of an MOF-based catalyst that exhibits synergetic effects in the oxidation of CO at moderate temperatures and the capture of CO_2 at low temperatures. The design strategy for this catalyst was based on the hypothesis that a cerium-based MOF could have a high affinity for oxygen because of the presence of cerium f orbitals

and could be able to store oxygen and enhance the catalytic oxidization of CO by Pd nanoparticles. The Ce-based MOF chosen for this study, namely, $\{[Ce(BTC)(H_2O)]\cdot DMF\}_n$ (where BTC is benzene-1,3,5-tricarboxylate and DMF is dimethylformamide), has a polymeric structure formed by the assembly of cerium metal clusters using the BTC as an organic linker.[27] The structure is marked by highly dense and homogeneously distributed cerium sites. The high affinity of these sites for oxygen provides an excellent opportunity to deposit an active CO oxidation catalyst such as Pd nanoparticles in regions where where CO molecules can be efficiently adsorbed.

Our approach to the synthesis of Pd/Ce-MOF is based on the simultaneous activation of the pores of the Ce-MOF and the rapid chemical reduction of the Pd precursor, namely, $Pd(NO_3)_2$. This can be achieved by the fast microwave-irradiation- (MWI-) assisted chemical reduction of the Pd ions using hydrazine hydrate as a reducing agent. The main advantage of MWI over other conventional heating methods is the rapid and uniform heating of the reaction mixture, which results in the fast reduction of the Pd ions with the simultaneous generation of a supersaturated solution of Pd atoms and the subsequent nucleation and growth of these atoms to form Pd nanoparticles within the pores and on the surface of the Ce-MOF crystals.[4,24,26,28,29] Furthermore, MWI heating can remove the coordinated DMF molecules around the Ce centers of the Ce-MOF crystals, thus generating a higher surface area and accessible pores for catalytic processes.[29]

■ RESULTS AND DISCUSSION

The as-prepared Ce-MOF crystals were obtained by filtration from the reaction mixture, washed with ethanol, and dried in a vacuum oven at 100 °C as colorless needle-shaped crystals. The XRD pattern of the Ce-MOF displayed in Figure 1 shows the
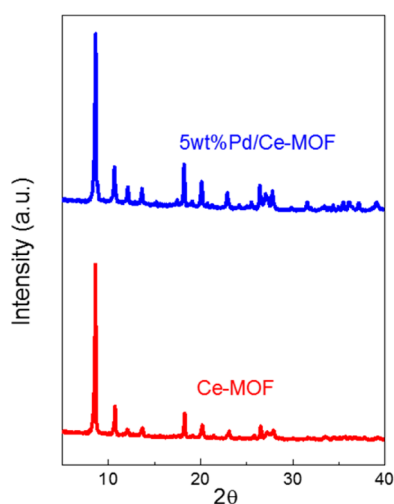
Figure 1. XRD patterns of Ce-MOF and 5 wt % Pd Ce-MOF.

characteristic peaks at (2θ) 8.4°, 10.6°, and 18.1°, indicating a high degree of crystallinity, in excellent agreement with the literature results.[30] The actual loading of the Pd nanoparticles on the Ce-MOF was determined by inductively coupled plasma mass spectrometry (ICP-MS) to be 4.93 wt %, in excellent agreement with the nominal loading of 5 wt % used in the preparation of the sample with the XRD pattern displayed in

Figure 1. The XRD pattern indicates that the incorporation of the Pd nanoparticles within the Ce-MOF crystals creates a supported catalyst without compromising the integrity of the Ce-MOF crystal structure.[30]

The Fourier transform infrared (FTIR) spectrum of the as prepared Ce-MOF crystals is presented in Figure 2. The spectrum shows the characteristic bands of the COO^- groups of BTC^{3-}, such as the 1612 cm^{-1} asymmetric vibration and the 1435 and 1373 cm^{-1} symmetric vibrations. In addition, low-intensity bands of the Ce−O stretching vibrations can be observed near 500−700 cm^{-1}. Also, the presence of DMF in the Ce-MOF crystals is evident from the band for C=O vibrations at 1666 cm^{-1}, indicating that the framework is stabilized by the presence of the strongly adsorbed solvent molecules. The strong OH stretching band of water at 3450 cm^{-1} is attributed to physically adsorbed water molecules on the surface of the Ce-MOF crystals.

The Raman spectrum of the Ce-MOF crystals is displayed in Figure 2b. The spectrum clearly shows the five characteristic sharp Raman bands at 826, 1006, 1450, 1550, and 1610 cm^{-1} assigned to out-of-plane ring C—H bending vibrations, C=C modes of the benzene ring, ν_{sym} of the $C-O_2$ units, ν_{asym} of the $C-O_2$ units, and C=C modes of the benzene ring, respectively, in agreement with the assignments reported in the literature.[31]

The morphology of the supported catalysts was characterized by transmission electron microscopy (TEM). It can be seen from Figure 3a,b that the Ce-MOF crystals had needle-shaped particles that ranged in size from 2 to 6 μm. Figure 3c,d displays TEM images of the 5 wt % Pd/Ce-MOF catalyst prepared by the microwave-assisted chemical reduction of palladium nitrate using hydrazine hydrate as the reducing agent. It is clear that this procedure resulted in the homogeneous distribution of the Pd nanoparticles across the Ce-MOF crystals. From the measured particle size distribution shown in Figure 3e, the Pd nanoparticles in the 5 wt % Pd/Ce-MOF catalyst had an average size of 4.6 ± 2.2 nm, which suggests that most of the particles were present on the surface of the Ce-MOF crystals.

To characterize the surface compositions of the Ce-MOF and the supported Pd catalysts, we carried out XPS measurements, as shown in Figure 4 for both the Pd 3d and Ce 3d electrons. The C 1s XPS spectra of the Ce-MOF support and the 5 wt % Pd/Ce-MOF catalyst are shown in Figure S1 (Supporting Information). The C 1s spectra show peaks corresponding to oxygen-containing groups between 285.5 and 289 eV, in addition to sp^2-bonded carbon C=C at 284.5 eV. Typically, peaks at 285.6, 286.7, 287.7, and 289 eV are assigned to the C 1s signals of C—OH, C—O, C=O, and HO—C=O groups, respectively.[29] The Ce 3d spectra of both the Ce-MOF support and the 5 wt % Pd/Ce-MOF supported catalyst show the presence of the Ce^{4+} 3d level characterized by four peaks corresponding to v and v′ $(3d^{5/2})$ (882.1 and 888.7 eV, respectively) and u and u′ $(3d^{3/2})$ (900.4 and 906.7 eV, respectively).[32] We also observed two peaks (doublet) at 885 and 904.1 eV, corresponding to v′ and u′, respectively, for Ce^{3+} 3d states.[33] The XPS spectra of the Pd 3d electron in the 5 wt % Pd/Ce-MOF catalyst show binding energies of 335.8 and 340.1 eV, indicating that the atomic-percentage ratio of Pd^0 to Pd^{2+} in the 5 wt % Pd/Ce-MOF was 1.37.[29] The presence of Pd^{2+} is attributed to the formation of a thin layer of PdO, which can act as a reservoir for oxygen that can be released during the CO oxidation reaction.
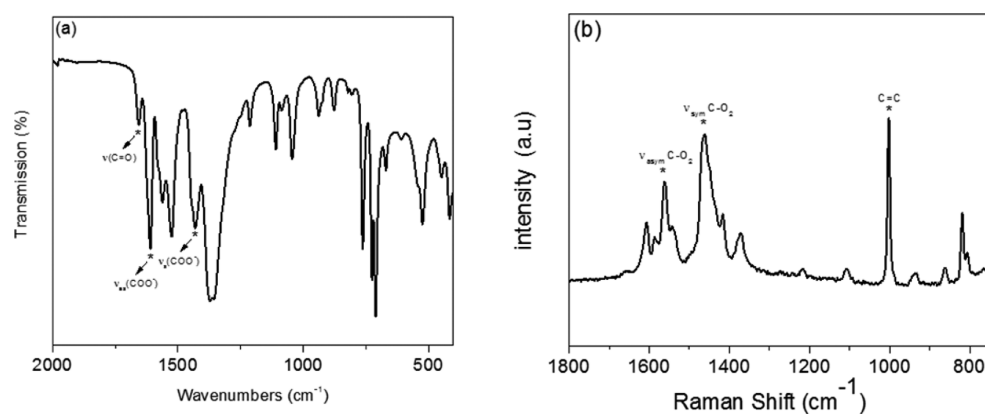
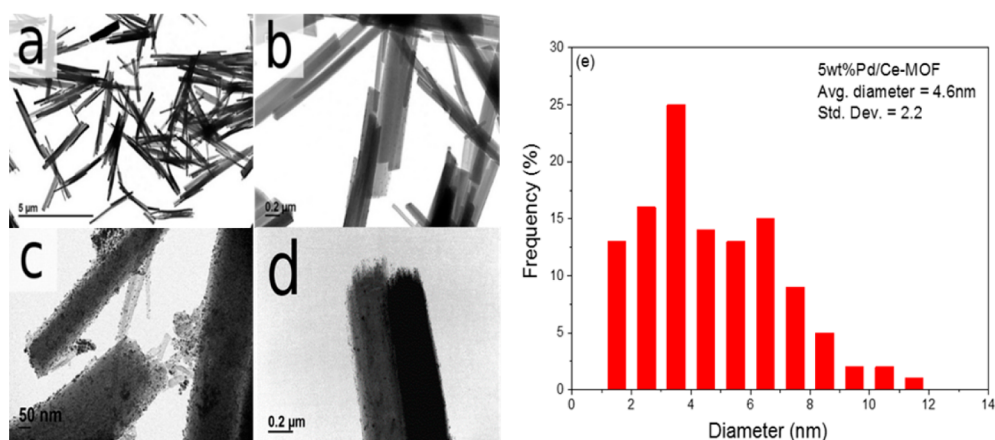**Figure 2.** (a) FTIR and (b) Raman spectra of Ce-MOF.

Figure 3. TEM images of (a,b) Ce-MOF crystals and (c,d) 5 wt % Pd/Ce-MOF catalyst. (e) Size distribution of the Pd nanoparticles in the 5 wt % Pd/Ce-MOF catalyst.
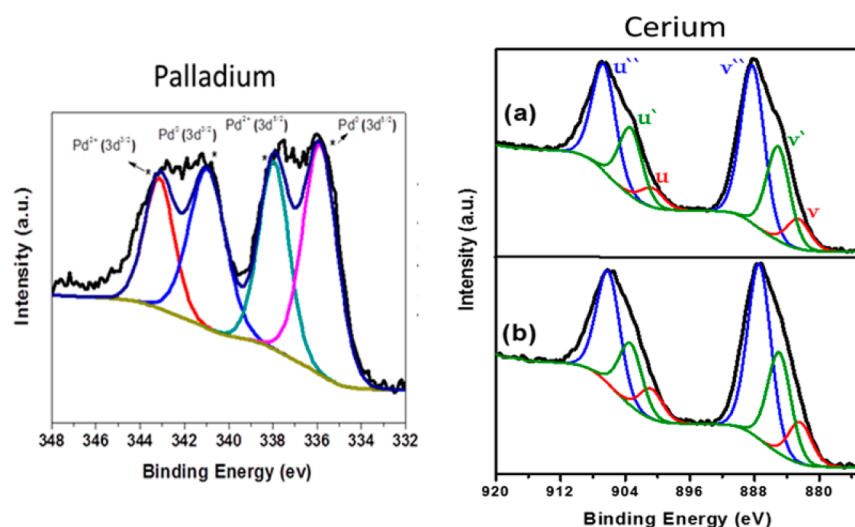

Figure 4. XPS spectra of (left) Pd 3d electrons in 5 wt % Pd/Ce-MOF catalyst and (right) Ce 3d electrons in (a) Ce-MOF and (b) 5 wt % Pd/Ce-MOF catalyst.

The thermal stability of the Ce-MOF was characterized by thermogravimetric analysis (TGA) in air, the results of which are shown in Figure 5. The TGA curve for the Ce-MOF is consistent with the literature results and shows the loss of adsorbed water and DMF over the temperature range of 150–250 °C, followed by framework decomposition at ~350 °C.[27] On the other hand, the TGA trace for the as-prepared 5 wt %

Pd/Ce-MOF catalyst shows only an initial weight loss of ~15 wt % due to water desorption at about 100 °C and significant catalyst decomposition at 500 °C. The TGA trace of the 5 wt % Pd/Ce-MOF catalyst indicates that the Pd loading process under MWI eliminates DMF from the pores of the Ce-MOF through exchange with water. It also suggests that the small Pd nanoparticles incorporated within the pores of the Ce-MOF
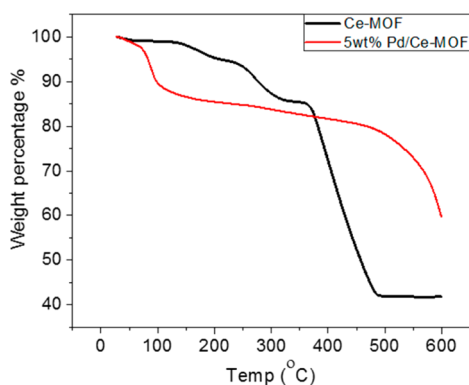
Figure 5. Comparison of the TGA plots of Ce-MOF and 5 wt % Pd/Ce-MOF.

provide an extra stabilizing effect against the collapse of the framework, as is evident by the significant increase in the decomposition temperature from ∼350 to 500 °C.

The N_2 gas sorption isotherms at −196 °C, shown in Figure 6a, reveal that the Ce-MOF had a small Brunauer−Emmett−Teller (BET) specific surface area of 62 m^2/g, consistent with the low porosity of this MOF and with previous measurements.[27,30] Interestingly, the surface area increased to 89 m^2/g for the 5 wt % Pd/Ce-MOF catalyst, indicating that the treatment of Ce-MOF under MWI during the reduction of the Pd ions by hydrazine hydrate resulted in the activation of the Ce-MOF, probably by removing impurities and unwanted species from the surface and pores of the MOF.

We considered the impact of loading Pd onto the Ce-MOF on the CO_2 uptake because of the contribution of CO_2 to global warming and because of its potential use as chemical feedstock. It has been observed that the loading of porous structures such as MOFs and high-surface-area graphite plates with Pd nanoparticles can have adverse effects on the gas uptake of these structures, which is very important for gas storage and separation, as well as for use in catalytic processes.[34] For example, it has been reported that the loading of a redox-active MOF with Pd nanoparticles resulted in an improvement in the hydrogen storage of the MOF but had the opposite effect on its CO_2 capture.[35] Whereas Pd nanoparticles provide effective sites for improved hydrogen interactions, the presence of other species such as counterions inside the pores of MOFs has been suggested to impede CO_2 uptake.[35,36]

The loading of Pd onto Ce-MOF (5 wt %) was found to lead to a significant improvement in the CO_2 uptake at 273 K, as

shown in Figure 6b. Table 1 reports the BET surface area and CO_2 uptake results for Ce-MOF and 5 wt % Pd/Ce-MOF.

Table 1. BET Surface Areas and CO_2 Uptakes at 273 K of Ce-MOF and 5 wt % Pd/Ce-MOF

material	BET surface area (m^2 g^{-1})	CO_2 uptake (mmol g^{-1})
Ce-MOF	62.2[a] (636[b])	1.7
5 wt % Pd/Ce-MOF	89.3[a] (620[b])	3.5

[a]Calculated from N_2 isotherms. [b]Obtained from CO_2 adsorption isotherms.

Whereas the pristine Ce-MOF had an uptake of only 1.7 mmol g^{-1} at 1.0 bar, the 5 wt % Pd/Ce-MOF exhibited an improved CO_2 capture capacity that reached 3.5 mmol g^{-1} under the same conditions. As can be seen in Figure 6b, the fully reversible CO_2 isotherm of Ce-MOF shows a pronounced hysteresis, which is most likely due to the fact that the ultranarrow pores of Ce-MOF have a strong affinity for CO_2 molecules yet only limited adsorption sites because of the low surface area of this MOF. On the other hand, loading of Pd onto Ce-MOF and its subsequent activation increased the surface area from 62 m^2/g for Ce-MOF to 89 m^2/g for the 5 wt % Pd/Ce-MOF and presumably provided additional adsorption sites for CO_2 on the surface of the Pd nanoparticles, as evidenced by the improved CO_2 uptake of 5 wt % Pd/Ce-MOF reported in Table 1 and the diminished hysteresis of the CO_2 isotherm of 5 wt % Pd/Ce-MOF shown in Figure 6b.

Despite their low N_2 uptakes at 77 K, Ce-MOF crystals show high CO_2 uptake values at 273 K, which is indicative of their microporosity.[37] The poor N_2 adsorption of the Ce-MOF can be attributed to the low diffusivity and adsorption kinetics of N_2 molecules at 77 K, which is due to the ultranarrow pores of the Ce-MOF.[37,38] Because of the substantial CO_2 uptake by ultramicroporous materials, the use of CO_2 as a probe for porosity measurements is preferred over the use of N_2.[37] Accordingly, we calculated the pore size distribution and surface area of the Ce-MOF using CO_2 adsorption isotherms collected at 273 K. As expected, our CO_2-based porosity measurements indicated a much higher surface area and smaller pores for the Ce-MOF when compared to our N_2-based porosity measurements, as shown in Table 1. It should be mentioned that the use of CO_2 isotherms of materials with high binding affinities for CO_2 can lead to the overestimation of surface area values.[39] We also estimated the pore size distribution for 5 wt % Pd/Ce-MOF using nonlocal density
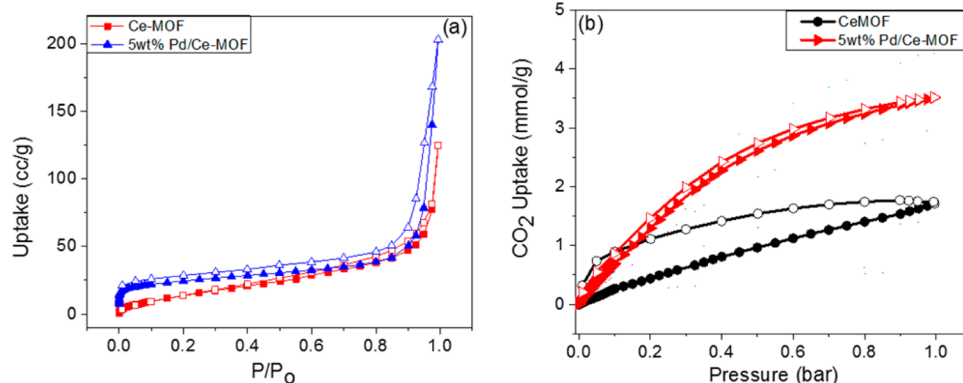
Figure 6. (a) N_2 gas sorption isotherms and (b) CO_2 uptakes of Ce-MOF and 5 wt % Pd/Ce-MOF.

functional theory (NLDFT)[39] with both the N_2 (7.3 Å) and CO_2 (5.4 Å) isotherms (Figure S2, Supporting Information), and in both cases, the pore size distribution values were in good agreement with reported channel dimensions of the Ce-MOF (6.6 × 6.6 Å).[27] The ability of the Ce-MOF to bind and release CO_2 during catalytic processes is very important to ensure sufficient mass transfer inside the pores. Later in this section, we demonstrate the remarkable activity of the 5 wt % Pd/Ce-MOF in the low-temperature oxidation of CO to CO_2.

The CO oxidation conversions for different Pd loadings incorporated within the Ce-MOF are shown in Figure 7. The
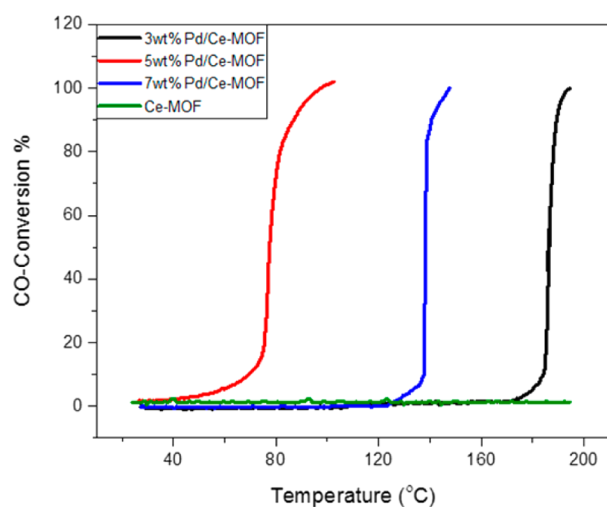
Figure 7. CO oxidation with different loadings of Pd as a function of temperature for a reactant gas mixture containing 4.0 wt % CO and 20.0 wt % O_2 in helium (25 mg of catalyst, flow rate of 100 cm^3/min).

CO oxidation conversion increased significantly as the Pd content was increased from 3 wt %, at which the 50% and 100% conversions occurred at 180 and 190 °C, respectively, to 5 wt %, at which these conversions occur at 77 and 92 °C, respectively. However, increasing the Pd loading to 7 wt % resulted in increasing the temperatures of the 50% and 100% conversion to 140 and 148 °C, respectively. This is probably due to the aggregation of the Pd nanoparticles on the surface of the Ce-MOF, which could result in a decrease of the surface area of the catalyst. It should also be noted that the Ce-MOF with no loading of Pd nanoparticles shows no activity for CO oxidation at temperatures below 200 °C. This confirms that the Pd nanoparticles supported on the Ce-MOF play the primary role in the oxidation process. The ability of cerium to store oxygen appears to enhance the oxidation process by creating oxygen vacancies, leading to enhanced activity.

We also considered loading the Ce-MOF with other metal nanoparticle catalysts such as Au and Pt using the same MWI-assisted chemical reduction procedure as used for the preparation of the Pd/Ce-MOF catalyst. Comparison of the oxidations of CO conducted on Ce-MOFs with 5 wt % loadings of Pd, Au, and Pt nanoparticles (Figure S3, Supporting Information) indicates that the 5 wt % Pd/Ce-MOF catalyst had the highest activity for CO oxidation. This could be due to the larger particle size and significant degrees of agglomeration of the Au and Pt catalysts prepared by the MWI method. The optimization of the synthesis procedures and loadings for the Au/Ce-MOF and Pt/Ce-MOF catalysts to obtain well-

dispersed small-nanoparticle catalysts for CO oxidation will be published elsewhere.[40]

Another attractive feature of the current Pd/Ce-MOF catalyst includes the long-term activity and stability of the catalyst, as no reduction in activity was observed after several repeated catalytic reaction cycles. Figure S4 (Supporting Information) shows no decrease in the 100% CO conversion provided by the 5 wt % Pd/Ce-MOF at 90 °C over a period of 8 h.

Comparison of the CO oxidation activity of the 5 wt % Pd/Ce-MOF with those of other nanoparticle catalysts supported on MOFs demonstrates the remarkable activity of the Pd/Ce-MOF supported catalyst. For example, a 5 wt % Au nanoparticle catalyst (4.2 nm) supported on ZIF-8 showed 50% CO conversion at 170 °C in comparison with 77 °C for the current 5 wt % Pd/Ce-MOF.[3] This significant difference in reactivity is even more remarkable when comparing the large surface area of ZIF-8 (1413 m^2/g)[3] to the much smaller value of 62 m^2/g for the current Ce-MOF support. This comparison clearly indicates that the enhanced activity of the Pd/Ce-MOF catalyst is due to the catalyst−support interaction of the Pd nanoparticles with the Ce centers of the support. Another piece of evidence for the specific role of the Pd−Ce interaction in enhancing the catalytic activity of the Pd/Ce-MOF catalyst comes from comparing the activity of the 1 wt % Pd catalyst supported on the MOF compound $Cu_3(BTC)_2$ with that of the current 5 wt % Pd/Ce-MOF catalyst.[19] The temperature for 100% CO conversion for the 1 wt % Pd/$Cu_3(BTC)_2$ catalyst is 205 °C, compared to 190 and 92 °C for the 3 wt % Pd/Ce-MOF and 5 wt % Pd/Ce-MOF, respectively, reported in this work. It should be noted that BTC is the same linker as used in the assembly of the Ce-MOF in this work, and therefore, the enhanced activity of the Pd-supported Ce-MOF appears to be more related to the Pd−Ce interaction than to the Pd−BTC interaction. This conclusion is also supported by the reactivity of a different metal catalyst such as the 5% Ag/$Cu_3(BTC)_2$ catalyst, which showed 100% CO conversion at 122 °C as compared to 92 °C for the 5 wt % Pd/Ce-MOF catalyst. The catalyst Co/MOF-74 showed catalytic activity with 50% CO conversion at 84 °C and 87% conversion at 130 °C.[41] However, this catalyst was unstable, and the framework collapsed after being heated above 150 °C in air and eventually transformed into Co_3O_4 at 230 °C.[41]

Table 2 summarizes the catalytic activities for CO oxidation of several MOF-supported catalysts. These data clearly demonstrate that the Pd/Ce-MOF catalyst prepared in this work exhibits a unique activity for CO oxidation in comparison with different types of MOF-based catalysts. This unique activity is attributed to the synergy between the Pd nano-

Table 2. Comparison of CO Oxidations on Metal-Supported MOF Catalysts

wt % Metal (ref)	MOF	$T_{50\%}$[a] (°C)	$T_{100\%}$[b] (°C)
5% Au[3]	ZIF-8	170	210
2.7% Pd[21]	MIL-53 (Al)	100	115
5% Ag[20]	$Cu_3(BTC)_2$	100	120
1% Pd[19]	$Cu_3(BTC)_2$	190	205
2.9% Pd[4]	MIL-101(Cr)	92	107
5% Pd (this work)	Ce-MOF	77	96

[a]Temperature for 50% conversion of CO into CO_2. [b]Temperature for 100% conversion of CO into CO_2.

particles and the Ce sites in the Ce-MOF, which leads to an enhanced activity for CO oxidation. This conclusion is consistent with the improved catalytic activity for CO oxidation found for Ce-modified Cu-MOF HKUST-1 $[Cu_3(BTC)_2(H_2O)_3 \cdot xH_2O]$.[42] However, the relatively higher activity of that catalyst (complete conversion of CO at 150 °C) was attributed to the formation of $CuO-CeO_2$ catalysts, which are known to exhibit good activity for CO oxidation.[43,44] In the present Pd/Ce-MOF system, there is no evidence for the formation of CeO_2, as the XRD pattern of the spent catalyst showed that the crystalline structures of Ce-MOF was maintained after several repeated cycles of CO oxidation. Therefore, the high activity of the Pd/Ce-MOF catalyst is most likely due to the interaction of the Pd nanoparticles and the Ce sites within Ce-MOF. One possible explanation for this activity could be due to electron transfer from the Pd nanoparticles to the Ce^{4+} cations, leading to the formation of Ce^{3+}, and subsequent electron transfer from Ce^{3+} to the adsorbed O_2 at the Pd/Ce-MOF interface, thus promoting the formation of active oxygen species for CO oxidation. A similar mechanism was suggested to explain the high activity of Pd/CeO_2 catalysts for low-temperature CO oxidation.[45]

CONCLUSIONS

In conclusion, we have developed a facile, general, and effective approach based on microwave irradiation for the incorporation of Pd nanoparticle catalyst within Ce-MOF. The resulting Pd/Ce-MOF is a unique catalyst that is capable of both CO oxidation at modest temperatures (370 K) and efficient uptake of the product CO_2 gas at low temperatures (273 K). The observed catalytic activity toward CO oxidation is significantly higher than those of other reported metal nanoparticles supported on metal−organic frameworks. The high activity of the Pd/Ce-MOF catalyst is attributed to the presence of Ce(III) and Ce(IV) ions within the metal−organic framework support. Pd nanoparticles supported on the Ce-MOF store oxygen in the form of a thin palladium oxide layer at the particle−support interface, in addition to the oxygen stored on the Ce(III)/Ce(IV) centers. Oxygen from these reservoirs can be released during CO oxidation at 373 K. At lower temperatures (273 K), the Pd/Ce-MOF has a significant CO_2 uptake of 3.5 mmol/g. An application for the Pd/Ce-MOF material could be suggested in two separate CO conversion and CO_2 storage devices operating at 370 and 273 K, respectively.

EXPERIMENTAL SECTION

Starting Materials. Dimethylformamide (DMF) and ethanol were purchased from Alfa Aesar. Cerium(III) nitrate hexahydrate, trimesic acid (H_3BTC), palladium(II) nitrate, and hydrazine hydrate were obtained from Sigma-Aldrich. All chemicals were used without further purification.

Synthesis of the Supported Catalysts. Synthesis of Ce-MOF was based on the following procedure:[27] First, 4.04 g of cerium(III) nitrate hexahydrate (10.0 mmol) and 1.40 g of trimesic acid (6.67 mmol) were sealed into a 100 mL Teflon-lined hydrothermal synthesis autoclave and heated to 100 °C for 24 h with 60 mL of DMF. The resulting white crystalline powder was extracted and washed twice with hot ethanol to remove unreacted reactants and excess DMF and then dried in a vacuum oven at 100 °C for 24 h. After recrystallization, palladium nitrate was loaded into 100 mg of the Ce-MOF in 40 mL of deionized water and stirred for 1 h. The palladium ions were reduced using hydrazine hydrate (80 μL) under MWI using a 700 W microwave oven for 90 s (in 10-s intervals). The supported catalyst

was washed twice with 40 mL of ethanol and then dried in a vacuum oven at 100 °C for 24 h.

Characterization of the Catalysts. The crystallinity of the catalysts was characterized by powder X-ray diffraction (XRD) using an X'Pert Philips materials research diffractometer. The patterns were obtained using copper radiation (Cu Kα, λ = 1.5405 Å) with a second monochromator at 45 kV and 40 mA at a scanning speed of 2° (2θ)/min. FTIR spectra of calcined samples were obtained using a Nicolet-Nexus 670 FTIR spectrophotometer (4 cm^{-1} resolution and 32 scans) in dried KBr (Sigma) pellets over a measuring range of 400−4000 cm^{-1}. Raman spectra were obtained using the Thermo Scientific DXR SmartRaman instrument with a 532-nm excitation wavelength. Transmission electron microscopy (TEM) images were obtained using a JEOL JEM-1230 microscope operated at 120 kV. For TEM images, the sample powder was dispersed in methanol using ultrasonic radiation for 10 min, and a drop of the suspension was placed onto a carbon-coated grid for TEM imaging. Gas sorption experiments were performed using a Quantachrome Autosorb iQ volumetric analyzer with adsorbates of ultrahigh-purity (UHP) grade. In a typical experiment, a sample of polymer (∼50 mg) was loaded into a 9-mm large bulb cell (Quantachrome) of known weight that was then connected to a gas analyzer and degassed at 150 °C and 1.0×10^{-5} bar for 10 h. The degassed sample was refilled, weighed precisely, and then transferred back to the analyzer. The temperatures for adsorption measurements were controlled using a refrigerated bath of liquid nitrogen (77 K) for N_2 and a temperature-controlled water bath (273 K) for CO_2. The surface electronic states were investigated by X-ray photoelectron spectroscopy (XPS; Thermo VG ESCALAB250 using Al Kα radiation). The XPS data were internally calibrated, fixing the binding energy of C 1s at 284.6 eV. Thermogravimetric analysis was carried out on a TGA Q5000 apparatus from TA Instruments.

CO Catalytic Oxidation. For oxidation experiments, the catalyst (25 mg) was placed inside a Thermolyne 2100 programmable tube furnace reactor (Figure S5, Supporting Information).[24−26] The sample temperature was measured with a thermocouple placed near the sample. In a typical experiment, a gas mixture consisting of 4 wt % CO and 20 wt % O_2 in helium was passed over the sample as the temperature was ramped. The gas mixture was set to flow over the sample at a rate of 100 cm^3/min controlled by MKS digital flow meters. The conversion of CO to CO_2 was monitored using an infrared gas analyzer (ACS, Automated Custom Systems Inc.). All catalytic activities were measured after heat treatment of the catalyst at 110 °C in the reactant gas mixture for 15 min to remove moisture and adsorbed impurities.

ASSOCIATED CONTENT

ⓢ Supporting Information

The Supporting Information is available free of charge on the ACS Publication Web site at The Supporting Information is available free of charge on the ACS Publications website at DOI: 10.1021/acsami.7b03555.

Carbon 1s XPS spectra of Ce-MOF and 5 wt % Pd/Ce-MOF; pore size distributions of 5 wt % Pd/Ce-MOF calculated using the N_2 and CO_2 adsorption isotherms at 77 K; comparison of CO oxidations on 5 wt % Pd/Ce-MOF, 5 wt % Au/Ce-MOF, and 5 wt % Pt/Ce-MOF; CO oxidation on 5 wt % Pd/Ce-MOF as a function of time at 90 °C for 8 h; and experimental setup for the catalytic oxidation of CO (PDF)

AUTHOR INFORMATION

Corresponding Author
*E-mail: mselshal@vcu.edu.

ORCID ⓘ
M. Samy El-Shall: 0000-0002-1013-4948

Notes

The authors declare no competing financial interest.

REFERENCES

(1) O'Keeffe, M.; Yaghi, O. M. Deconstructing the Crystal Structures of Metal−Organic Frameworks and Related Materials into Their Underlying Nets. *Chem. Rev.* **2012**, *112*, 675−702.

(2) Furukawa, H.; Cordova, K. E.; O'Keeffe, M.; Yaghi, O. M. The Chemistry and Applications of Metal−Organic Frameworks. *Science* **2013**, *341*, 974−986.

(3) Jiang, H. L.; Liu, B.; Akita, T.; Haruta, M.; Sakurai, H.; Xu, Q. Au@ZIF-8: CO Oxidation over Gold Nanoparticles Deposited to Metal−Organic Framework. *J. Am. Chem. Soc.* **2009**, *131*, 11302−11303.

(4) El-Shall, M. S.; Abdelsayed, V.; Khder, A. E. R. S.; Hassan, H. M. A.; El-Kaderi, H. M.; Reich, T. E. Metallic and Bimetallic Nanocatalysts Incorporated into Highly Porous Coordination Polymer MIL-101. *J. Mater. Chem.* **2009**, *19*, 7625−7631.

(5) Guo, Z.; Xiao, C.; Maligal-Ganesh, R. V.; Zhou, L.; Goh, T. W.; Li, X.; Tesfagaber, D.; Thiel, A.; Huang, W. Pt Nanoclusters Confined within Metal−Organic Framework Cavities for Chemoselective Cinnamaldehyde Hydrogenation. *ACS Catal.* **2014**, *4*, 1340−1348.

(6) Choi, K. M.; Na, K.; Somorjai, G. A.; Yaghi, O. M. Chemical Environment Control and Enhanced Catalytic Performance of Platinum Nanoparticles Embedded in Nanocrystalline Metal−Organic Frameworks. *J. Am. Chem. Soc.* **2015**, *137*, 7810−7816.

(7) Kitagawa, S.; Kitaura, R.; Noro, S. Functional Porous Coordination Polymers. *Angew. Chem., Int. Ed.* **2004**, *43*, 2334−2375.

(8) Hermes, S.; Schroter, M. K.; Schmid, R.; Khodeir, L.; Muhler, M.; Tissler, A.; Fischer, R. W.; Fischer, R. A. Metal@MOF: loading of highly porous coordination polymers host lattices by metal−organic chemical vapor deposition. *Angew. Chem., Int. Ed.* **2005**, *44*, 6237−6241.

(9) Perles, J.; Iglesias, M.; Martin-Luengo, M. A.; Monge, M. A.; Ruiz-Valero, C.; Snejko, N. Metal−Organic Scandium Framework: Useful Material for Hydrogen Storage and Catalysis. *Chem. Mater.* **2005**, *17*, 5837−5842.

(10) Sabo, M.; Henschel, A.; Froede, H.; Klemm, E.; Kaskel, S. Solution Infiltration of Palladium into MOF-5: Synthesis, Physisorption and Catalytic Properties. *J. Mater. Chem.* **2007**, *17*, 3827−3832.

(11) Dhakshinamoorthy, A.; Opanasenko, M.; Cejka, J.; Garcia, H. Metal−Organic Frameworks as Heterogeneous Catalysts for the Production of Fine Chemicals. *Catal. Sci. Technol.* **2013**, *3*, 2509−2540.

(12) Corma, A.; Garcia, H.; Llabres i Xamena, F. X. Engineering Metal−Organic Frameworks for Heterogeneous Catalysis. *Chem. Rev.* **2010**, *110*, 4606−4655.

(13) Morozan, A.; Jaouen, F. Metal−Organic Frameworks for Electrochemical Applications. *Energy Environ. Sci.* **2012**, *5*, 9269−9290.

(14) Li, S.-L.; Xu, Q. Metal−Organic Frameworks as Platforms for Clean Energy. *Energy Environ. Sci.* **2013**, *6*, 1656−1683.

(15) Fateeva, A.; Chater, P. A.; Ireland, C. P.; Tahir, A. A.; Khimyak, Y. Z.; Wiper, P. V.; Darwent, J. R.; Rosseinsky, M. J. A Water-Stable Porphyrin-Based Metal−Organic Framework Active for Visible-Light Photocatalysis. *Angew. Chem., Int. Ed.* **2012**, *51*, 7440−7444.

(16) Wang, C.; Xie, Z.; deKrafft, K. E.; Lin, W. Doping Metal−Organic Frameworks for Water Oxidation, Carbon Dioxide Reduction, and Organic Photocatalysis. *J. Am. Chem. Soc.* **2011**, *133*, 13445−13454.

(17) Zou, R.-Q.; Sakurai, H.; Xu, Q. Preparation, Adsorption Properties, and Catalytic Activity of 3D Porous Metal−Organic Frameworks Composed of Cubic Building Blocks and Alkali-Metal Ions. *Angew. Chem., Int. Ed.* **2006**, *45*, 2542−2546.

(18) Zou, R.-Q.; Sakurai, H.; Han, S.; Zhong, R.-Q.; Xu, Q. Probing the Lewis Acid Sites and CO Catalytic Oxidation Activity of the Porous Metal−Organic Polymer [Cu(5-methylisophthalate)]. *J. Am. Chem. Soc.* **2007**, *129*, 8402−8403.

(19) Ye, J.-Y.; Liu, C.-J. $Cu_3(BTC)_2$: CO Oxidation Over MOF based Catalysts. *Chem. Commun.* **2011**, *47*, 2167−2169.

(20) Zhao, Y.; Zhong, C.; Liu, C.-J. Enhanced CO Oxidation over Thermal treated Ag/Cu-BTC. *Catal. Commun.* **2013**, *38*, 74−76.

(21) Qian, L.; Zhen, Z.; Jian, L.; Yue-Chang, W.; Gui-Yuan, J.; Ai-Jun, D. Pd Nanoparticles Deposited on Metal−Organic Framework of MIL-53(Al): An Active Catalyst for CO Oxidation. *Acta Phys.-Chim. Sin.* **2014**, *30*, 129−134.

(22) Green, F.; Short, S. *IEH Assessment on Indoor Air Quality in the Home: Carbon Monoxide*; Institute for Environment and Health: Leicester, U.K., 1998.

(23) Igarashi, H.; Fujino, T.; Watanabe, M. Hydrogen Electro-Oxidation on Platinum Catalysts in the Presence of Trace Carbon Monoxide. *J. Electroanal. Chem.* **1995**, *391*, 119−123.

(24) Glaspell, G.; Hassan, H. M. A.; Elzatahry, A.; Abdalsayed, V.; El-Shall, M. S. Nanocatalysis on Supported Oxides for CO Oxidation. *Top. Top. Catal.* **2008**, *47*, 22−31.

(25) Yang, Y. L.; Saoud, K. M.; Abdelsayed, V.; Glaspell, G.; Deevi, S.; El-Shall, M. S. Vapor Phase Synthesis of Supported Pd, Au, and Unsupported Bimetallic Nanoparticle Catalysts for CO Oxidation. *Catal. Commun.* **2006**, *7*, 281−284.

(26) Glaspell, G.; Hassan, H. M. A.; Elzatahry, A.; Fuoco, L.; Radwan, N. R. E.; El-Shall, M. S. Nanocatalysis on Tailored Shape Supports: Au and Pd Nanoparticles Supported on MgO Nanocubes and ZnO Nanobelts. *J. Phys. Chem. B* **2006**, *110*, 21387−2193.

(27) Almáši, M.; Zelenak, V.; Opanasenko, M.; Cisarova, I. Ce(III) and Lu(III) Metal−Organic Frameworks with Lewis Acid Metal Sites: Preparation, Sorption Properties and Catalytic Activity in Knoevenagel Condensation. *Catal. Today* **2015**, *243*, 184−194.

(28) Jhung, S. H.; Lee, J.; Yoon, J. W.; Serre, C.; Férey, G.; Chang, J. Microwave Synthesis of Chromium Terephthalate MIL-101 and Its Benzene Sorption Ability. *Adv. Mater.* **2007**, *19*, 121−124.

(29) Ibrahim, A. A.; Lin, A.; Zhang, F.; Abouzeid, K. M.; El-Shall, M. S. Palladium Nanoparticles Supported on a Metal−Organic Framework-Partially Reduced Graphene Oxide Hybrid for the Catalytic Hydrodeoxygenation of Vanillin as a Model for Biofuel Upgrade Reactions. *ChemCatChem* **2017**, *9*, 469−480.

(30) Khan, N. A.; Haque, M. M.; Jhung, S. H. Accelerated Syntheses of Porous Isostructural Lanthanide−Benzenetricarboxylates (Ln−BTC) Under Ultrasound at Room Temperature. *Eur. J. Inorg. Chem.* **2010**, *2010* (31), 4975−4981.

(31) He, L.; Dumee, L. F.; Liu, D.; Velleman, L.; She, F.; Banos, C.; Davies, J. B.; Kong, L. Silver Nanoparticles Prepared by Gamma Irradiation across Metal−Organic Framework Templates. *RSC Adv.* **2015**, *5*, 10707−10715.

(32) Zhang, F.; Wang, P.; Koberstein, J.; Khalid, S.; Chan, S.-W. Cerium Oxidation State in Ceria Nanoparticles Studied with X-ray Photoelectron Spectroscopy and Absorption Near Edge Spectroscopy. *Surf. Sci.* **2004**, *563*, 74−82.

(33) Kar, S.; Patel, C.; Santra, S. Direct Room Temperature Synthesis of Valence State Engineered Ultra-Small Ceria Nanoparticles: Investigation on the Role of Ethylenediamine as a Capping Agent. *J. Phys. Chem. C* **2009**, *113*, 4862−4867.

(34) Sutradhar, N.; Sinhamahapatra, A.; Pahari, S.; Jayachandran, M.; Subramanian, B.; Bajaj, H. C.; Panda, A. B. Facile Low-Temperature Synthesis of Ceria and Samarium-Doped Ceria Nanoparticles and Catalytic Allylic Oxidation of Cyclohexene. *J. Phys. Chem. C* **2011**, *115*, 7628−7637.

(35) Adhikari, A. K.; Lin, K.-S. Improving CO_2 Adsorption Capacities and CO_2/N_2 Separation Efficiencies of MOF-74(Ni, Co) by Doping

Palladium-containing Activated Carbon. *Chem. Eng. J.* **2016**, *284*, 1348−1360.

(36) Cheon, Y. E.; Suh, M. P. Enhanced Hydrogen Storage by Palladium Nanoparticles Fabricated in a Redox-Active Metal−Organic Framework. *Angew. Chem., Int. Ed.* **2009**, *48*, 2899−2903.

(37) Mishra, A. K.; Ramaprabhu, S. Palladium Nanoparticles Decorated Graphite Nanoplatelets for Room Temperature Carbon Dioxide Adsorption. *Chem. Eng. J.* **2012**, *187*, 10−15.

(38) Moon, S.-Y.; Bae, J.-S.; Jeon, E.; Park, J.-W. Organic Sol−Gel Synthesis: Solution-Processable Microporous Organic Networks. *Angew. Chem., Int. Ed.* **2010**, *49*, 9504−9508.

(39) Kaur, P.; Hupp, J. H.; Nguyen, S. T. Porous Organic Polymers in Catalysis: Opportunities and Challenges. *ACS Catal.* **2011**, *1*, 819−835.

(40) Lin, A.; Ibrahim, A. A.; El-Shall, M. S. Gold and Platinum Nanoparticles Incorporated within Ce-Metal−Organic Framework for CO Oxidation. Unpublished results

(41) Kim, T.; Kim, D. H.; Kim, S.; Kim, Y. D.; Bae, Y.-S.; Lee, C. Y. Low-Temperature CO Oxidation Using a Metal−Organic Framework with Unsaturated Co^{2+}. *Polyhedron* **2015**, *90*, 18−22.

(42) Zamaro, J. M.; Perez, N. C.; Miro, E. E.; Casado, C.; Seoane, B.; Tellez, C.; Coronas, J. HKUST-1 MOF: A Matrix to Synthesize CuO and $CuO-CeO_2$ Nanoparticle Catalysts for CO Oxidation. *Chem. Eng. J.* **2012**, *195−196*, 180−187.

(43) Rao, K. N.; Bharali, P.; Thrimurthulu, G.; Reddy, B. M. Supported Copper−Ceria Catalysts for Low Temperature CO Oxidation. *Catal. Commun.* **2010**, *11*, 863−866.

(44) Mai, H.; Zhang, D.; Shi, L.; Yan, T.; Li, H. Highly Active $Ce_{1-x}Cu_xO_2$ Nanocomposite Catalysts for the Low Temperature Oxidation of CO. *Appl. Surf. Sci.* **2011**, *257*, 7551−7559.

(45) Liu, B.; Liu, J.; Li, T.; Zhao, Z.; Gong, X.-Q.; Chen, Y.; Duan, A.; Jiang, G.; Wei, Y. Interfacial Effects of CeO_2-Supported Pd Nanorod in Catalytic CO Oxidation: A Theoretical Study. *J. Phys. Chem. C* **2015**, *119*, 12923−12934.